NASA TM X-53062

AN AUTOMATED MODEL FOR PREDICTING AEROSPACE DENSITY BETWEEN 200 AND 60,000 KILOMETERS ABOVE THE SURFACE OF THE EARTH

by ROBERT E. SMITH
  Aero-Astrodynamics Laboratory

NASA

George C. Marshall
Space Flight Center,
Huntsville, Alabama

AN AUTOMATED MODEL FOR PREDICTING AEROSPACE DENSITY BETWEEN 200 AND 60,000 KILOMETERS ABOVE THE SURFACE OF THE EARTH

By

Robert E. Smith

George C. Marshall Space Flight Center

Huntsville, Alabama

ABSTRACT

297 28

This paper describes the derivation of a computer routine for predicting the vertical distribution of aerospace density in the terrestrial space environment above the surface of the earth. Solar activity, geomagnetic storm, diurnal heating, latitude, and the earth's orbital eccentricity effects are included in this model. Densities can be predicted for any time through December 1992.

Author

NASA - GEORGE C. MARSHALL SPACE FLIGHT CENTER

Technical Memorandum X-53062

AN AUTOMATED MODEL FOR PREDICTING AEROSPACE DENSITY BETWEEN 200 AND 60,000 KILOMETERS ABOVE THE SURFACE OF THE EARTH

By

Robert E. Smith

SPACE ENVIRONMENT GROUP
AERO-ASTROPHYSICS OFFICE
AERO-ASTRODYNAMICS LABORATORY
RESEARCH AND DEVELOPMENT OPERATIONS

TABLE OF CONTENTS

LIST OF ILLUSTRATIONS

DEFINITION OF SYMBOLS

Symbol	Definition
$f(t)$	correction factor for diurnal heating effect
$F_{10.7}$	altitude variation of solar flux variability correction factor
$m(Z)$	altitude variation of correction factor for diurnal heating effect
S_Y	annual mean value of 10.7 centimeter solar radio noise flux $(\times 10^{-22}$ Watts per Meter^2 per Cycle per Second)
S_F	monthly mean value of 10.7 centimeter solar radio noise flux $(\times 10^{-22}$ Watts per Meter^2 per Cycle per Second)
SS	annual mean sunspot number
Z	altitude in kilometers
ρ	density of aerospace gas in kilograms per cubic meter

AN AUTOMATED MODEL FOR PREDICTING AEROSPACE DENSITY BETWEEN 200 AND 60,000 KILOMETERS ABOVE THE SURFACE OF THE EARTH

SUMMARY

What space environmental conditions may be expected for an early morning launch at Cape Kennedy, Florida, in September 1972, an afternoon launch in March 1983, or an evening launch in July 1990? Designers of space vehicles and their co-workers in the fields of trajectory optimization, orbital lifetime prediction, and mission analysis and evaluation need the answers to these questions today to insure an economical, safe, successful, and smoothly integrated space program. This paper attempts to provide the answer to one aspect of this problem through a fully automated, predictive model of the density-height profile in that part of the terrestrial space environment from 200 to 60,000 kilometers above the earth's surface.

A set of analytical expressions for computing time and solar flux dependent density-height profiles in the upper atmosphere above the earth's surface is derived from an analysis of current observations [8, 17, 26]. Admittedly the available data sample is far from adequate; however, data requirements of using agencies have made the development of a predictive model of paramount importance.

A forecast is made of the solar activity expected during the twentieth and twenty-first solar cycles. The results are used in the prediction of density-height profiles during these solar cycles.

The accuracy of the predictions for the distant future depends to a great extent upon the subjective predictions of the twentieth and twenty-first solar cycles. The solar cycle predictions can be updated periodically as the nineteenth solar cycle progresses, thereby improving the overall accuracy of the density predictions.

Values of atmospheric density predicted using this system of equations are compared in Figure 1 with the 1959 ARDC Standard Atmosphere and the 1962 U. S. Standard Atmosphere.

INTRODUCTION

During the early horse-and-buggy days of space travel, meteorologists were called upon to furnish current information as well as relatively short range predictions of atmospheric parameters within the confines of the troposphere; however, as vehicles were refined and improved, the upper boundary of the region for which information was required was pushed from the troposphere through the tropopause into the stratosphere. With the advent of jet-type aircraft, missiles, and finally orbiting manned and unmanned spacecraft, the upper limit was extended even farther from the surface of the earth - from the homosphere to the heterosphere [20] - the time limit was extended to several days, and the personnel who provided the required information were now called aerospace technologists rather than meteorologists. Soon the boundaries will be removed once again, to cislunar and translunar space with time durations of several months, and in the not too distant future one can foresee interplanetary and possibly intergalactic travel with associated prediction requirements of several years duration.

With each transition the provision of adequate data has become increasingly difficult with the transition from the homosphere to the heterosphere having the greatest magnitude, for preliminary results from theoretical considerations and rocket-borne experiments soon revealed that here was an entirely new and radically different realm. In this outermost region, the heterosphere, the rules and relationships which had been established to explain the behavior of the homosphere would not always produce the results observed. Such familiar basic equations as the perfect gas law and the hydrostatic equation were not applicable, unreservedly [20], to this tenuous gas plasma which was not mixed but stratified, which was not always in hydrostatic equilibrium [27], and whose composition was not only highly variable and contained charged as well as neutral particles but also could not be accurately measured with existing instrumentation. New observational techniques as well as new and more sophisticated instrumentation had to be developed. While great improvements have been made, complete success is still in the distant future.

Despite the scarcity of verified theories and observational data, requirements for data of greater scope as well as higher accuracy and reliability for use in more refined design criteria, trajectory optimization, and orbital lifetime predictions continue to increase with no sign of abatement. One aerospace parameter for which the demand is particularly great is the vertical distribution of atmospheric density - the density-height profile - and its temporal and spatial variability. While there is no intention of slighting or underestimating the importance of temperature, molecular weight, pressure, and composition and the temporal and spatial distribution and variability of each, this paper will present an

independent, completely automated, predictive model of the vertical distribution of density in that portion of the terrestrial space environment from 200 to 60,000 kilometers above the earth's surface based on the criteria established in Section II.

In the immediate future a model for the transition region between 90 and 200 kilometers above the earth's surface will be developed which will mesh with the Patrick AFB, Florida Reference Atmosphere* developed by Mr. O. E. Smith, Marshall Space Flight Center and this model for the region above 200 kilometers.

Following that development, future research activity will be directed toward the identification and separation of the geomagnetic and latitude effects [6, 26], now included in Equations 4a and 4b, and the development of specific corrective factors for each of these effects on density [3, 9, 10, 11] for inclusion in this model.

I wish to express my thanks to Miss Sylvia Bowers of the computations section for her invaluable assistance in programming this system of equations on the GE 225 computer.

II. DISCUSSION

An intensive literature survey was undertaken to determine the current state-of-the-art knowledge of the density-height profile in the terrestrial space environment. Terrestrial space is here defined as the region from 130 to 60,000 kilometers above the surface of the earth. A multitude of theoretical models [20] have been advanced, some based purely on hypothesis, some based on a few widely scattered satellite [1, 8, 17, 26] and rocket-borne observations [2, 6, 13, 18] combined with theoretical explanations derived from solutions to problems of the homosphere, and some based on basic principles. From this survey it was determined that a representative model of the density-height profile of the terrestrial space environment above 100 kilometers above the earth's surface should incorporate the following features:

1. Time- and latitude-dependent density at any specific altitude between 200 and 60,000 kilometers [1, 6, 7, 14, 16, 20, 21].

2. A diurnal heating effect such that the density is a minimum at approximately 0600 LST (Local Standard Time) and a maximum at 1400 LST above 180 kilometers and a maximum at approximately 0600 LST and a minimum at 1400 LST between 120 and 180 kilometers [1, 7, 9, 10, 11, 14, 15, 16, 18, 20, 23, 25].

3. A maximum diurnal variation in density between 500 and 700 kilometers above the earth's surface [9, 24].

4. No diurnal variation in density below 120 kilometers [7, 11, 14, 20].

5. A solar activity dependent density at any altitude between 100 and 1200 kilometers with the 10.7 centimeter solar radio noise flux being used as an indicator for the amount of solar activity [1, 9, 10, 11, 14, 15, 16, 19, 24].

Although they are not specifically evident in the final set of equations, the following additional features were considered in the development of the model:

1. A constant mean molecular weight and composition below 105 ± 5 kilometers [14, 16, 20, 21], and a time and solar flux dependent mean molecular weight above 105 ± 5 kilometers [16, 19, 21].

2. Complete mixing of the gases below and diffusive equilibrium above 105 ± 5 kilometers [7, 12, 16, 20].

III. PROCEDURES

From the literature survey it was determined that a system wherein a series of corrections could be applied, when needed, to a basic expression for the vertical distribution of density at a certain time of the day under a specific solar radio noise flux was the most feasible approach since each portion of the final set of equations could be updated individually whenever newer data dictated. Equation 1 below is the basic expression. The subscripts in this and all future expressions in this paper are of the form (time of day, amount of 10.7 centimeter solar radio noise flux, altitude). Equations 2 and 3 contain the corrective factors with $f(t)$ being the correction for the time of day or diurnal heating effect, $m(Z)$ providing the correction for the altitude variation of the diurnal heating effect, and $F_{10.7}$ $(S_F - 25)$ providing the correction due to the variation in the 10.7 centimeter solar radio noise flux.

Equation 1 was derived through a least squares fit to a combination of observed [8, 17, 26] and empirical data adjusted to 0600 LST (Local Standard Time) for a period of absolute minimum solar flux, $S_F = 25 \times 10^{-22}$ watts per meter^2 per cycle per second [28].

$$\log \rho_{(06,25,Z)} = \frac{200.0 - Z}{51.654467 + 0.10790209Z} - 10.28. \qquad (1)$$

Equation 3 will produce the density at any altitude, Z, at any time of the day, t_L, and at any level of solar activity, S_F.

$$\log \rho_{(06,S_F,Z)} = \log \rho_{(06,25,Z)} + F_{10.7} (S_F - 25) \qquad (2)$$

$$\rho_{(t_L,S_F,Z)} = \rho_{(06,S_F,Z)} [1 + f(t) \ m(Z)]. \qquad (3)$$

The next step was the development of a corrective factor which would make the model dependent upon the amount of incoming solar radiation. A preliminary analysis of values of density derived from satellite orbit analyses showed that no single correction factor could be derived to fit the range of fluctuations at the various altitudes; therefore, two equations were derived which would produce an envelope whose range would cover the range of the observed values. It is realized that the equations developed in this manner mask, among other effects, the geomagnetic storm and latitude effects as well as accounting for the fact that the 10.7 centimeter solar flux is not a perfect indicator of solar activity [2]. Insufficient information, however, precludes the separation of these three effects at this time. It is hoped that this distinction can be made soon as more observational data become available. Equation 4a will produce the lower limit curve, while Equation 4b will produce the upper limit curve for the predicted density for any solar activity.

$$F_{10.7} = 10^{-2} \sum_{i=0}^{6} A_i \cos i\lambda + B_i \sin i\lambda, \qquad (4a)$$

where

$A_0 = 0.29333333$

$A_1 = 0.12981833$ $B_1 = 0.32333268$

$A_2 = -0.1137500$ $B_2 = -0.93819375 \times 10^{-2}$

$A_3 = 0.25833333 \times 10^{-1}$ $B_3 = -0.32500000 \times 10^{-1}$

$A_4 = 0.79166666 \times 10^{-2}$ $B_4 = -0.21650625 \times 10^{-2}$

$A_5 = 0.14348333 \times 10^{-1}$ $B_5 = 0.21667316 \times 10^{-1}$

$A_6 = -0.17500000 \times 10^{-1}$

$$F_{10.7} = 10^{-2} \sum_{p=0}^{6} C_p \cos p\lambda + D_p \sin p\lambda, \qquad (4b)$$

where

$C_0 = 0.44583333$

$C_1 = 0.17221255$ $\qquad\qquad$ $D_1 = 0.41152230$

$C_2 = -0.83333333 \times 10^{-1}$ $\qquad$ $D_2 = -0.41857866 \times 10^{-1}$

$C_3 = 0.66666666 \times 10^{-2}$ $\qquad$ $D_3 = -0.16666666 \times 10^{-2}$

$C_4 = 0.21666666 \times 10^{-1}$ $\qquad$ $D_4 = -0.15877102 \times 10^{-1}$

$C_5 = -0.38792000 \times 10^{-2}$ $\qquad$ $D_5 = 0.21811050 \times 10^{-1}$

$C_6 = -0.91666666 \times 10^{-2}$

and

$$\lambda = \left(\frac{700 - Z}{100}\right) \frac{\pi}{6}$$

for $200 \leq Z = 1200$ km and $F_{10.7} = 0.0000$ for $Z > 1200$ kilometers.

Equation 5 will produce the diurnal bulge specified in feature #2 of Section II.

$$f(t) = 10^{-3} \sum_{i=0}^{12} a_i \cos it + b_i \sin it, \qquad (5)$$

where

$$a_0 = 469.166 \qquad a_7 = 4.488 \qquad b_1 = 67.804 \qquad b_7 = 1.450$$

$$a_1 = 468.764 \qquad a_8 = -1.666 \qquad b_2 = -77.152 \qquad b_8 = 0.000$$

$$a_2 = 116.638 \qquad a_9 = -4.212 \qquad b_3 = 1.818 \qquad b_9 = 3.484$$

$$a_3 = -36.622 \qquad a_{10}= 0.446 \qquad b_4 = 18.042 \qquad b_{10}= 0.068$$

$$a_4 = -18.750 \qquad a_{11}= 1.008 \qquad b_5 = 0.784 \qquad b_{11}= -3.698$$

$$a_5 = -0.928 \qquad a_{12}= -1.25 \qquad b_6 = -4.584$$

$$a_6 = 2.916$$

and $t = (t_L - 14.00)\ \pi/12$ and t_L = Local Standard Time on a twenty-four-hour clock.

The fifth step was the development of a corrective factor which, when combined with Equation 5, would produce the altitude variation in the diurnal bulge specified in feature #3, Section II. Assuming that the 10.7 centimeter solar radio noise flux remained essentially constant during the period from 0600 to 1400 LST, the times of the diurnal minimum and maximum, respectively, then Equation 3 could be solved from m(Z) for a series of values of Z by substituting appropriate values for

$$\rho_{(06,S_F,Z)} \quad \text{and} \quad \rho_{(14,S_F,Z)}$$

from available observational data knowing that $f(t) = 1$ when $t_L = 14.00$. These solutions of Equation 3 established a set of numbers [m, Z] from which Equations 6a and 6b were derived.

$$m(Z) = (-0.24125 \times 10^{-2} + 0.31125 \times 10^{-4}\ Z)\ (Z - 200.0) + 0.05 \tag{6a}$$

for

$$200 = Z < 600$$

$$m(Z) = \frac{Z - 600.0}{56.93259 - 0.15889906Z} + 6.50 \tag{6b}$$

for

$$600 = Z = 60,000.$$

7

To produce an entirely automated system, it was necessary to derive a second set of analytical expressions capable of predicting the solar activity parameter, S_F, used in Equation 2. Figure 2 shows yearly solar activity values in terms of smoothed mean Zurich sunspot numbers for the period from January 1749 through December 1962 [4].

Figure 3 is a composite overlay of solar cycles 2, 3, 4, and 5, while Figure 4 is the same overlay of solar cycles 18 and 19 with predictions for 20 and 21. These predictions are based on the observed similarities between the first recorded series of cycles (2, 3, 4, and 5) and the current series plus the following facts:

1. Over 200 years of recorded data (Figure 2) fail to show more than four increasing peaks in any sequence of solar cycles.

2. The first peak (fifth peak in any sequence) after any maximum peak is always greater than the peak (third in any sequence) preceding the maximum peak.

3. The second peak (sixth in any sequence) after any maximum peak is always substantially less than the five preceding peaks.

Figure 5 shows monthly mean values for the 10.7 centimeter solar radio noise flux as recorded at the National Research Council, Ottawa, Canada, for the period February 1947 through December 1961.

Figure 6 is a plot of the smoothed mean Zurich sunspot number versus monthly mean 10.7 centimeter solar flux during the period February 1947 through December 1961. A least squares fit to the smooth curve drawn on the graph produced the following equation, correct to ±10% [23], for computing a yearly mean value for the 10.7 centimeter solar flux parameter, S:

$$S_Y = \sum_{k=0}^{8} c_k \, SS^k, \tag{7}$$

where

$$c_0 = 67.80036 \qquad\qquad c_5 = -0.261604186 \times 10^{-8}$$

$$c_1 = 0.419498444 \qquad\qquad c_6 = -0.159036136 \times 10^{-10}$$

$$c_2 = 0.427501471 \times 10^{-2} \qquad c_7 = 0.140461971 \times 10^{-12}$$

$$c_3 = -0.469543503 \times 10^{-4} \qquad c_8 = -0.274461310 \times 10^{-15}$$

$$c_4 = 0.660862973 \times 10^{-6}$$

and SS = Zurich smoothed mean sunspot number.

Once the yearly mean value of the 10.7 centimeter solar radio noise flux has been predicted using Equation 7, Equations 8a and 8b will compute the monthly mean value that would be predicted if the earth's orbit about the sun were a perfect circle.

$$S_M = S_Y + (M - 6/12)(S_{Y+1} - S_Y) \qquad \text{for } M \geq 6 \qquad (8a)$$

$$S_M = S_Y - (6 - M/12)(S_Y - S_{Y-1}) \qquad \text{for } M < 6. $$

Das Gupta [5], however, presented observational data showing a semiannual variation [15, 17] in incident 10.7 centimeter solar flux due to the earth's orbital eccentricity. A reexamination of his data combined with a curve fit by a harmonic analysis of the new results produced the following equation which will correct the results obtained from Equations 8a and 8b above, for the semiannual variation and produce the final value of the solar activity parameter, S_F, to be used in Equation 2:

$$S_F = S_M \sum_{n=0}^{6} d_n \cos n\theta + e_n \sin n\theta, \qquad (8)$$

where

$$d_0 = 0.10000000 \times 10^1$$

$$d_1 = -0.28737186 \times 10^{-1} \qquad e_1 = -0.13090493 \times 10^{-1}$$

$$d_2 = -0.10333333 \times 10^{-1} \qquad e_2 = -0.12701714 \times 10^{-1}$$

$$d_3 = 0.15000000 \times 10^{-2} \qquad e_3 = -0.35000000 \times 10^{-2}$$

$$d_4 = -0.50000000 \times 10^{-3} \qquad e_4 = -0.20207273 \times 10^{-2}$$

$$d_5 = 0.20601563 \times 10^{-2} \qquad e_5 = -0.24095063 \times 10^{-2}$$

$$d_6 = 0.28333333 \times 10^{-2}$$

and $\theta = (M - 6)\,\pi/6$, and where M is a figure corresponding to the month of the year beginning with January = 1, February = 2, etc.

IV. ELECTRONIC DATA PROCESSING PROGRAM

The following program has been developed for use on a GE 225 computer. There are two options for input data. If the monthly mean value for the 10.7 centimeter solar radio noise flux is known or predicted, then option 1 is read into the machine and the input data consist of the time of day, t_L; 10.7 centimeter monthly mean solar radio flux, S_F; beginning altitude, BZ; ending altitude, EZ; and altitude increment, DZ. If the results are to be based on the known or predicted value of the annual smoothed mean Zurich sunspot number as determined from Figure 4, then option 2 is read into the machine and the input data consist of the month of the year, M; time of day, t_L; sunspot number, SS; and altitude, Z. If sense switch 19 is down, the output will be the maximum density predicted; however, if sense switch 19 is up, the output will be the minimum density predicted. In every instance, the output will consist of the time of day, 10.7 centimeter solar radio noise flux, altitude, and the predicted density.

200 AND 60000 KM ABOVE EARTHS SUZFACE
R.E. SMITH   JOB NUMBER

```
      COMMON FM(12),SC(9),SFD(7),SFE(7),FA(7),FB(7),FC(7),FD(7),FTA(13),
     1FTB(13)
      COMMON SS(30),SY(30)
      PI6=.52359878
      CONL=2.30258509
      FA=.29333333
      FA(2)=.12981833
      FA(3)=-.11375
      FA(4)=.25833333E-1
      FA(5)=.79166666E-2
      FA(6)=.14348333E-1
      FA(7)=-.175E-1
      FB=0.
      FB(2)=.32333268
      FB(3)=-.93819375E-2
      FB(4)=-.325E-1
      FB(5)=-.21650625E-2
      FB(6)=.21667316E-1
      FB(7)=0.
      FC=.44583333
      FC(2)=.17221255
      FC(3)=-.83333333E-1
      FC(4)=.66666666E-2
      FC(5)=.21666666E-1
      FC(6)=-.38792E-2
      FC(7)=-.91666666E-2
      FD=0.
      FD(2)=.4115223
      FD(3)=-.41857866E-1
      FD(4)=-.16666666E-1
      FD(5)=-.15877102E-1
      FD(6)=.2181105E-1
      FD(7)=0.
      FTA=469.166
      FTA(2)=466.764
      FTA(3)=116.638
      FTA(4)=-36.622
      FTA(5)=-18.75
      FTA(6)=-.928
      FTA(7)=2.916
      FTA(8)=4.488
      FTA(9)=-1.666
      FTA(10)=-4.212
      FTA(11)=.446
      FTA(12)=1.008
      FTA(13)=-1.25
      FTB=0.
      FTB(2)=67.304
      FTB(3)=-77.152
      FTB(4)=1.818
      FTB(5)=18.042
      FTB(6)=.784
      FTB(7)=-4.584
```

11

```
        FTB(8)=1.45
        FTB(9)=0.
        FTB(10)=3.484
        FTB(11)=.068
        FTB(12)=-3.698
        FTB(13)=0.
        SC=67.60036
        SC(2)=.419498444
        SC(3)=.427501471E-2
        SC(4)=-.469543503E-4
        SC(5)=.660862973E-6
        SC(6)=-.261604186E-8
        SC(7)=-.159036136E-10
        SC(8)=.140461971E-12
        SC(9)=-.27446131E-15
        SFD=1.
        SFD(2)=-.28737186E-1
        SFD(3)=-.10333333E-1
        SFD(4)=.15E-2
        SFD(5)=-.5E-3
        SFD(6)=.20601563E-2
        SFD(7)=.28333333E-2
        SFE=0.
        SFE(2)=-.13090493E-1
        SFE(3)=-.12701714E-1
        SFE(4)=-.35E-2
        SFE(5)=-.20207273E-2
        SFE(6)=-.24095063E-2
1       RCD,IOP
IOP IS INPUT OPTION
        IF(SENSE SWITCH 19)2,4
2       PRINT 3
3       FORMAT (1H1,30HF 10.7 COMPUTED BY EQUATION 4B),
        GO TO 6
4       PRINT 5
5       FORMAT (1H1,30HF 10.7 COMPUTED BY EQUATION 4A)
6       CONTINUE
        GO TO (10,20),IOP
10      RCD,TL,SF,BZ,EZ,DZ
        GO TO 40
20      RCD,NM,NS,TL,Z,(FM(I),I=1,NM),(SS(K),K=1,NS)
        DO 25 K=1,NS
        SY(K)=SC
        DO 24 I=2,9
24      SY(K)=SC(I)*SS(K)**(I-1)+SY(K)
25      CONTINUE
        DO 105 K=1,NS
        DO 100 I=1,NM
        IF(FM(I)-6.)30,35,35
M LESS THAN 6
30      IF(K-1)31,31,32
31      SM=SY(K)
        GO TO 38
32      SM=SY(K)-((6.-FM(I))/12.*(SY(K)-SY(K-1)))
        GO TO 38
```

```
 35      IF(K-N5)37,36,36
 36      SM=SY(K)
         GO TO 38
 37      SM=SY(K)+((FM(I)-6.)/12.*(SY(K+1)-SY(K)))
 38      TM=(FM(I)-6.)*PI6
         SF=SFD
         DO 39 L=2,7
         FL=L-1
         FL=FL*TM
 39      SF=SF+SFD(L)*COSF(FL)+SFE(L)*SINF(FL)
         SF=SM*SF
 40      PRINT 410
 410     FORMAT (3X/////)
         T=(TL-14.)*PI6/2.
         FT=FTA
         DO 41 L=2,13
         FL =L-1
         FL=FL*T
 41      FT=FT+FTA(L)*COSF(FL)+FTB(L)*SINF(FL)
         FT=FT*1.0E-3
         IF(Z-600.)42,43,43
 42      FMZ=(-.24125E-2+.31125E-4*Z)*(Z-200.)+.05
         GO TO 44
 43      FMZ=(Z-600.)/(56.93259-.15889006*Z)+6.5
 44      IF(Z-1200.)50,50,45
 45      F107=0.
         GO TO 70
 50      FLAM=(700.-Z)*PI6/100.
         IF(SENSE SWITCH 19)60,51
```

```
 51      F107=FA
         DO 55 L=2,7
         FL=L-1
         FL=FL*FLAM
 55      F107=F107+FA(L)*COSF(FL)+FB(L)*SINF(FL)
         F107=F107/100.
         GO TO 70
```

```
 60      F107=FC
         DO 61 L=2,7
         FL=L-1
         FL=FL*FLAM
 61      F107=F107+FC(L)*COSF(FL)+FD(L)*SINF(FL)
         F107=F107/100.
 70      RHO1=(200.-Z)/(51.654457+.10790209*Z)-10.28
         RHO2=(RHO1+F107*(SF-25.))*CONL
         RHO2=EXPF(RHO2)
         RHO3=RHO2*(1.+FT*FMZ)
         PRINT 81,TL,Z,SF,RHO3
 81      FORMAT (2HTLE17.9,3X1HZE17.9,3X2HSFE17.9,3X2HR3E17.9)
         GO TO(85,90),IOP
 85      Z=Z+DZ
         IF(Z-EZ)40,40,1
 90      PRINT 91,SS(K),FM(I)
 91      FORMAT (2HSSE17.9,3X1HME17.9)
```

```
100    CONTINUE
105    CONTINUE
       GO TO 1
       END
```

V. RESULTS

Figure 1 is a plot of the 1959 ARDC Standard Atmosphere, 1962 U. S. Standard Atmosphere, and values predicted by this system for a 10.7 centimeter solar radio noise flux of 150×10^{-22} watts per meter^2 per cycle per second at 0900 LST. The envelope developed by this system encompasses the values for both the 1959 and 1962 standard atmospheres from ~320 to 580 kilometers, the region in this model in which both the diurnal and solar activity effects on the density are the greatest.

Table I shows the diurnal variation of the density-height profile at a 10.7 centimeter solar radio noise flux of 100×10^{-22} watts per meter^2 per cycle per second while Table II shows the diurnal variation at a 10.7 centimeter flux of 250×10^{-22} watts per meter^2 per cycle per second. The amplitude of the diurnal variation is greatest between 500 and 700 kilometers above the surface of the earth.

Table III shows the variation of the density-height profile with solar activity, S_F, at a constant time of 0900 LST. The amplitude of the variation due to solar activity is greatest between 300 and 400 kilometers above the earth's surface.

Figure 7 shows the envelopes of density variation at 200 and 600 kilometers above the earth's surface during the period July 1964 through December 1992 at 0600 LST and 1400 LST.

TABLE I

DIURNAL VARIATION OF DENSITY-HEIGHT PROFILE

ALT	0600 LST		0900 & 2200 LST		1400 LST	
KM	MIN $(Density - kg/m^3)$	MAX	MIN $(Density - kg/m^3)$	MAX	MIN $(Density - kg/m^3)$	MAX
200	8.810E-11	1.245E-10	9.031E-11	1.276E-10	9.251E-11	1.307E-10
300	8.757E-12	1.237E-11	1.201E-11	1.696E-11	1.526E-11	2.156E-11
400	1.652E-12	2.334E-12	3.352E-12	4.735E-12	5.052E-12	7.137E-12
500	2.248E-13	3.344E-13	6.737E-13	1.002E-12	1.123E-12	1.670E-12
600	4.400E-14	6.489E-14	1.870E-13	2.758E-13	3.300E-13	4.867E-13
700	1.106E-14	1.589E-14	3.682E-14	5.291E-14	6.258E-14	8.994E-14
800	3.429E-15	4.733E-15	9.716E-15	1.337E-14	1.599E-14	2.201E-14
900	1.272E-15	1.539E-15	3.190E-15	3.858E-15	5.108E-15	6.177E-15
1000	5.589E-16	6.146E-16	1.279E-15	1.407E-15	1.999E-15	2.199E-15
1100	2.805E-16	2.878E-16	5.971E-16	6.128E-16	9.137E-16	9.377E-16
1200	1.582E-16		3.176E-16		4.769E-16	
1500	4.278E-17		7.570E-17		1.086E-16	
2000	9.772E-18		1.531E-17		2.085E-17	
2500	3.665E-18		5.345E-18		7.025E-18	
3000	1.822E-18		2.535E-18		3.247E-18	
3500	1.080E-18		1.453E-18		1.826E-18	
4000	7.191E-19		9.436E-19		1.168E-18	
4500	5.197E-19		6.688E-19		8.180E-19	
5000	3.986E-19		5.050E-19		6.115E-19	
5500	3.195E-19		3.997E-19		4.800E-19	
6000	2.650E-19		3.281E-19		3.912E-19	
6500	2.258E-19		2.771E-19		3.284E-19	
7000	1.965E-19		2.393E-19		2.821E-19	
7500	1.741E-19		2.106E-19		2.471E-19	
8000	1.564E-19		1.881E-19		2.198E-19	
8500	1.422E-19		1.702E-19		1.982E-19	
9000	1.306E-19		1.556E-19		1.806E-19	
9500	1.210E-19		1.435E-19		1.661E-19	
10000	1.129E-19		1.334E-19		1.540E-19	
15000	7.223E-20		8.345E-20		9.466E-20	
20000	5.748E-20		6.564E-20		7.381E-20	
25000	5.003E-20		5.674E-20		6.345E-20	
30000	4.557E-20		5.145E-20		5.733E-20	
35000	4.262E-20		4.796E-20		5.330E-20	
40000	4.053E-20		4.549E-20		5.046E-20	
45000	3.896E-20		4.365E-20		4.834E-20	
50000	3.775E-20		4.223E-20		4.671E-20	
55000	3.679E-20		4.110E-20		4.542E-20	
60000	3.600E-20		4.018E-20		4.436E-20	

100

$(x10^{-22} w/m^2-c-s$ units of 10.7 cm solar radio noise flux)

TABLE II

DIURNAL VARIATION OF DENSITY-HEIGHT PROFILE

ALT	0600 LST		0900 & 2200 LST		1400 LST	
KM	MIN (Density - kg/m^3)	MAX	MIN (Density - kg/m^3)	MAX	MIN (Density - kg/m^3)	MAX
200	2.483E-10	6.998E-10	2.545E-10	7.173E-10	2.607E-10	7.348E-10
300	5.853E-11	1.650E-10	8.026E-11	2.262E-10	1.020E-10	2.874E-10
400	2.711E-11	7.641E-11	5.500E-11	1.550E-10	8.289E-11	2.336E-10
500	1.980E-12	6.520E-12	5.936E-12	1.954E-11	9.892E-12	3.257E-11
600	2.309E-13	7.408E-13	9.814E-13	3.148E-12	1.732E-12	5.556E-12
700	3.579E-14	1.062E-13	1.191E-13	3.537E-13	2.025E-13	6.011E-13
800	7.352E-15	1.917E-14	2.077E-14	5.417E-14	3.419E-14	8.916E-14
900	1.926E-15	3.405E-15	4.829E-15	8.538E-15	7.732E-15	1.367E-14
1000	6.759E-16	8.987E-16	1.547E-15	2.057E-15	2.418E-15	3.215E-15
1100	2.954E-16	3.193E-16	6.288E-16	6.797E-16	9.623E-16	1.040E-15
1200	1.582E-16		3.176E-16		4.769E-16	
1500	4.278E-17		7.570E-17		1.086E-16	
2000	9.772E-18		1.531E-17		2.085E-17	
2500	3.665E-18		5.345E-18		7.025E-18	
3000	1.822E-18		2.535E-18		3.247E-18	
3500	1.080E-18		1.453E-18		1.826E-18	
4000	7.191E-19		9.436E-19		1.168E-18	
4500	5.197E-19		6.688E-19		8.180E-19	
5000	3.986E-19		5.050E-19		6.115E-19	
5500	3.195E-19		3.997E-19		4.800E-19	
6000	2.650E-19		3.281E-19		3.912E-19	
6500	2.258E-19		2.771E-19		3.284E-19	
7000	1.965E-19		2.393E-19		2.821E-19	
7500	1.741E-19		2.106E-19		2.471E-19	
8000	1.564E-19		1.881E-19		2.198E-19	
8500	1.422E-19		1.802E-19		1.982E-19	
9000	1.306E-19		1.556E-19		1.806E-19	
9500	1.210E-19		1.435E-19		1.661E-19	
10000	1.129E-19		1.334E-19		1.540E-19	
15000	7.223E-20		8.345E-20		9.466E-20	
20000	5.748E-20		6.564E-20		7.381E-20	
25000	5.003E-20		5.674E-20		6.346E-20	
30000	4.557E-20		5.145E-20		5.733E-20	
35000	4.262E-20		4.796E-20		5.330E-20	
40000	4.053E-20		4.549E-20		5.046E-20	
45000	3.896E-20		4.365E-20		4.834E-20	
50000	3.775E-20		4.223E-20		4.671E-20	
55000	3.679E-20		4.110E-20		4.542E-20	
60000	3.600E-20		4.018E-20		4.436E-20	

250

$(x10^{-22}w/m^2-c-s$ units of 10.7 cm solar radio noise flux)

TABLE III

DENSITY-HEIGHT PROFILE VARIATION WITH SOLAR ACTIVITY AT 0900 LST

ALT	100*		150*		200*		250*	
KM	MIN (Density - kg/m³)	MAX	MIN (Density - kg/m³)	MAX	MIN (Density - kg/m³)	MAX	MIN (Density - kg/m³)	MAX
200	9.031E-11	1.276E-10	1.276E-10	2.268E-10	1.802E-10	4.034E-10	2.545E-10	7.173E-10
300	1.201E-11	1.696E-10	2.262E-11	4.022E-11	4.261E-11	9.593E-11	8.026E-11	2.262E-10
400	3.352E-12	4.735E-12	8.519E-12	1.515E-11	2.165E-11	4.846E-11	5.500E-11	1.550E-10
500	6.737E-13	1.002E-12	1.392E-12	2.698E-12	2.874E-12	7.261E-12	5.936E-12	1.954E-11
600	1.870E-13	2.758E-13	3.250E-13	6.210E-13	5.647E-13	1.398E-12	9.814E-13	3.148E-12
700	3.682E-14	5.291E-14	5.446E-14	9.967E-14	8.055E-14	1.877E-13	1.191E-13	3.537E-13
800	9.716E-15	1.337E-14	1.252E-14	2.132E-14	1.612E-14	3.398E-14	2.077E-14	5.417E-14
900	3.190E-15	3.858E-15	3.663E-15	5.027E-15	4.206E-15	6.552E-15	4.829E-15	8.538E-15
1000	1.279E-15	1.407E-15	1.363E-15	1.596E-15	1.452E-15	1.812E-15	1.547E-15	2.057E-15
1100	5.971E-16	6.128E-16	6.075E-16	6.343E-16	6.181E-16	6.565E-16	6.288E-16	6.797E-16
1200	3.176E-16	3.176E-16	3.176E-16	3.176E-16	3.176E-16	3.176E-16	3.176E-16	3.176E-16
1500	1.531E-17	1.531E-17	1.531E-17	1.531E-17	1.531E-17	1.531E-17	1.531E-17	1.531E-17

Densities above 1200 kilometers above the surface of the earth are independent of solar activity.

* 10.7 cm solar flux times 10⁻²² watts per meter squared per cycle per second.

Fig. 1. Comparison of 1959 ARDC Standard Atmosphere, 1964 U. S. Standard Atmosphere and Comparable Atmosphere Predicted by This Model
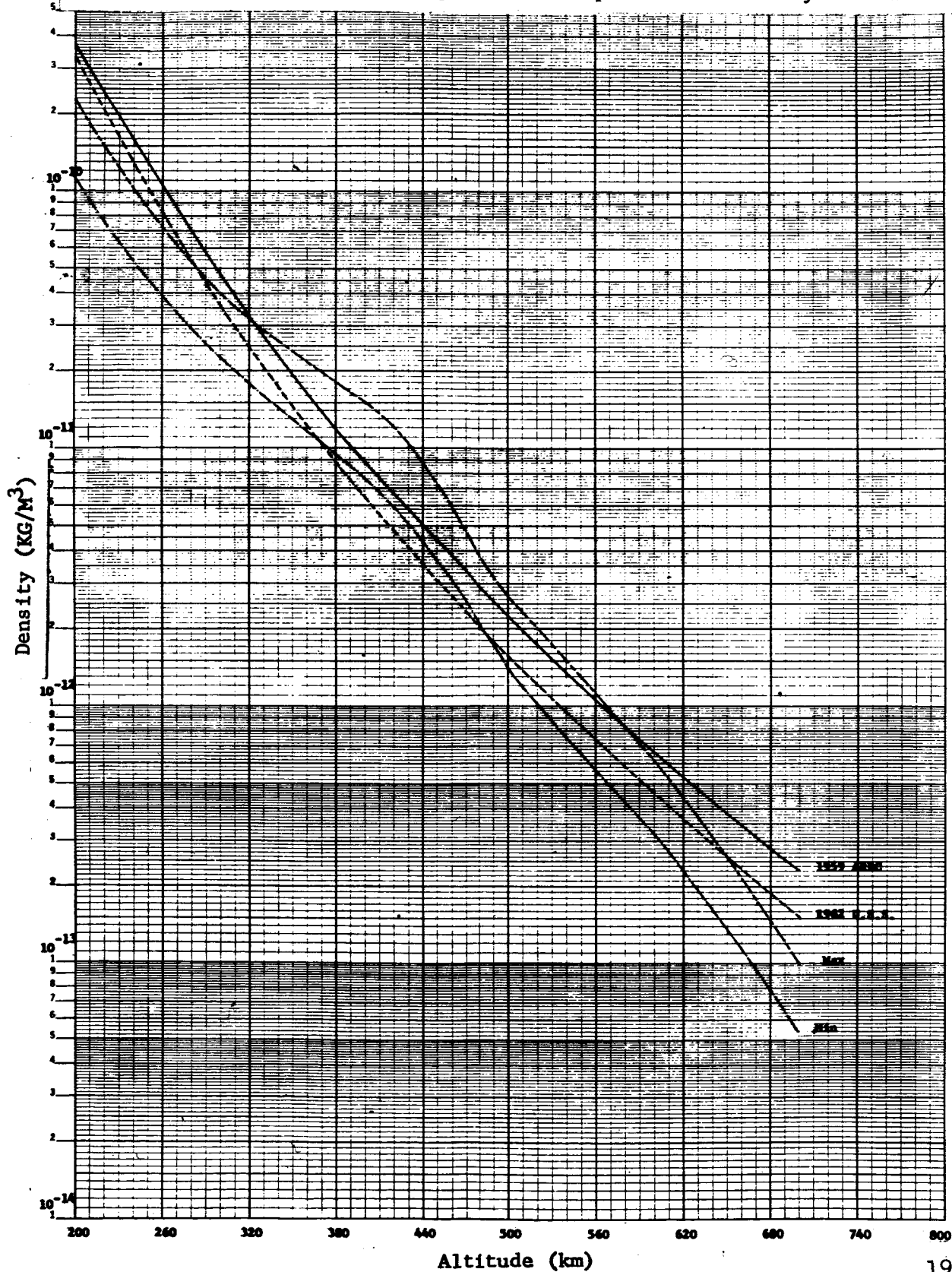
19

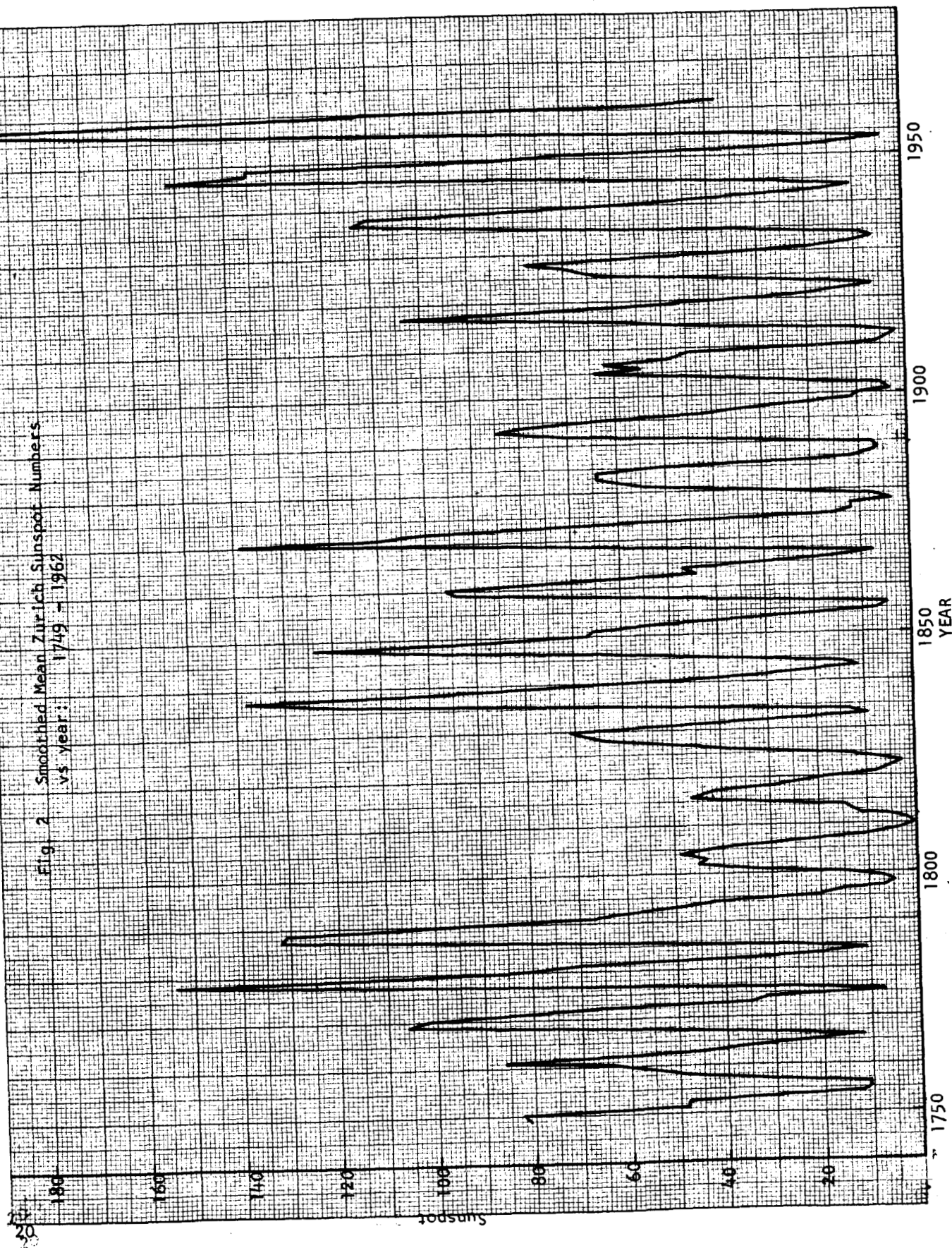Fig. 2 Smoothed Mean Zurich Sunspot Numbers vs Year: 1749 - 1962

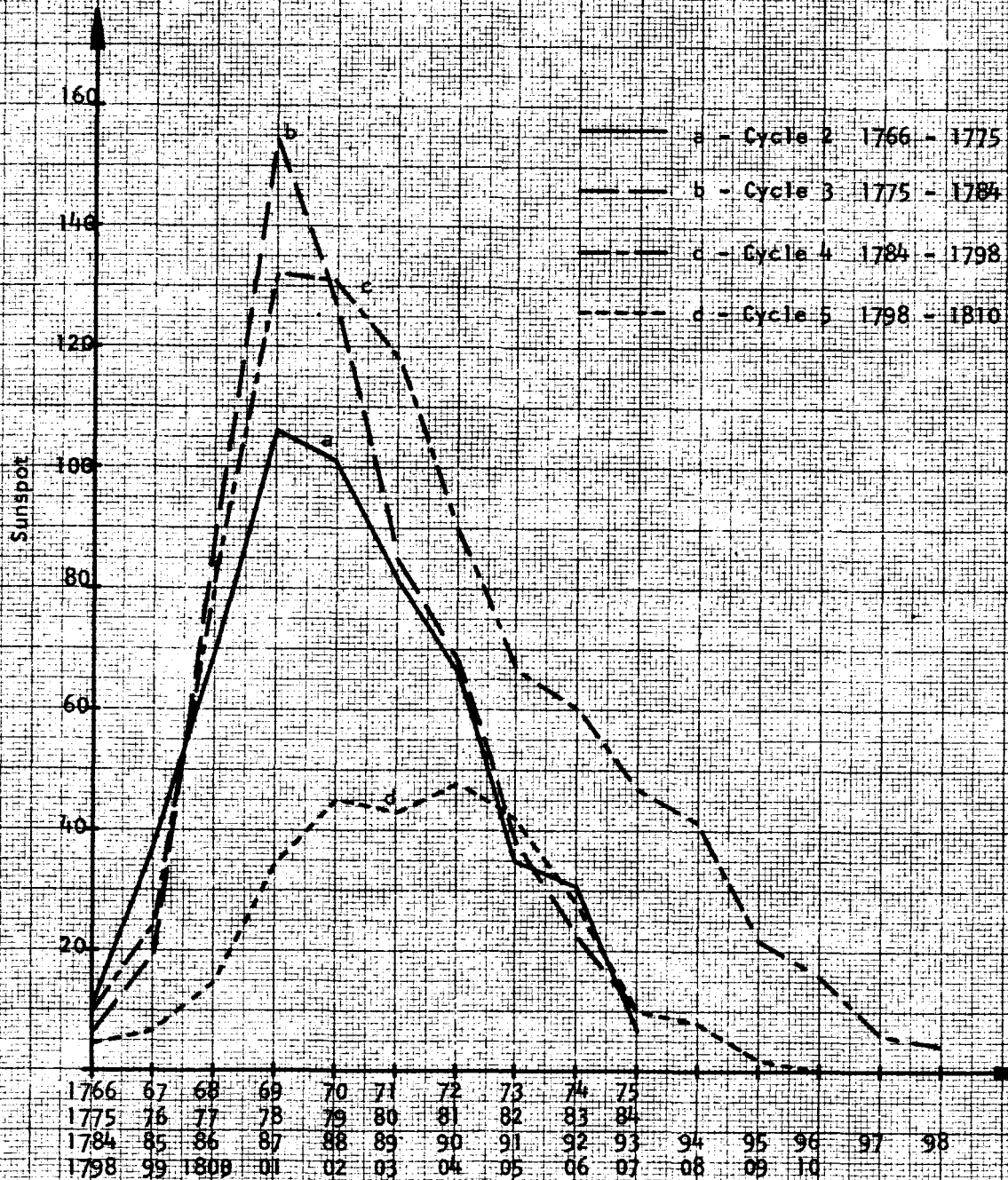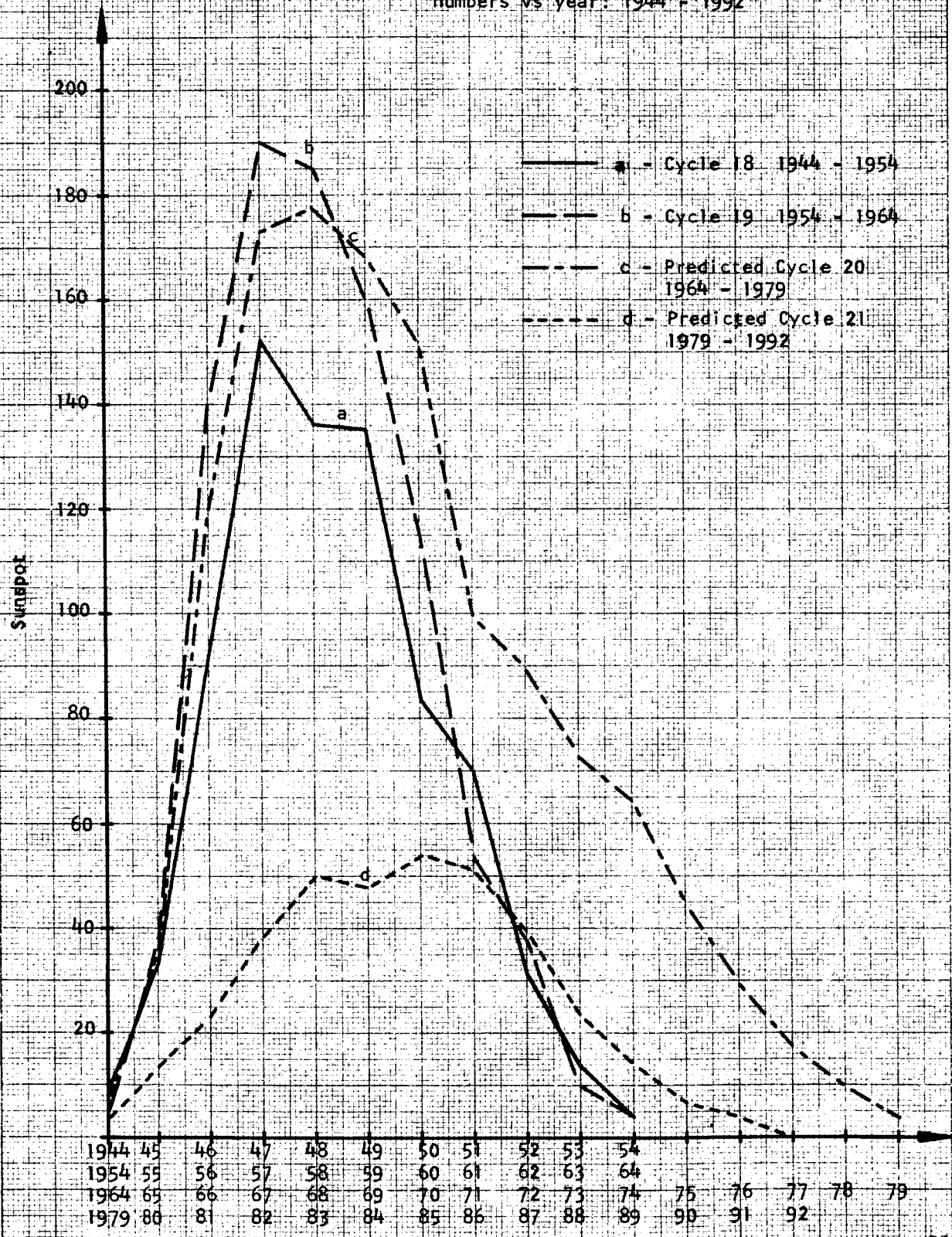Fig. 3 Smoothed Mean Zurich Sunspot Numbers vs Year: 1766 - 1810

a — Cycle 2   1766 - 1775
b — Cycle 3   1775 - 1784
c — Cycle 4   1784 - 1798
d — Cycle 5   1798 - 1810

Fig. 4 Smoothed Mean Zurich Sunspot
numbers vs year: 1944 – 1992

a – Cycle 18 1944 – 1954
b – Cycle 19 1954 – 1964
c – Predicted Cycle 20
1964 – 1979
d – Predicted Cycle 21
1979 – 1992

Sunspot

200
180
160
140
120
100
80
60
40
20

1944	45	46	47	48	49	50	51	52	53	54				
1954	55	56	57	58	59	60	61	62	63	64				
1964	65	66	67	68	69	70	71	72	73	74	75	76	77	78	79
1979	80	81	82	83	84	85	86	87	88	89	90	91	92	

22

Fig. 5 Mean 2800 MC Radio Noise vs Month
February 1947 - December 1961

10.7 Cm Solar Flux (x10⁻²² w/m²/c/s)

YEAR
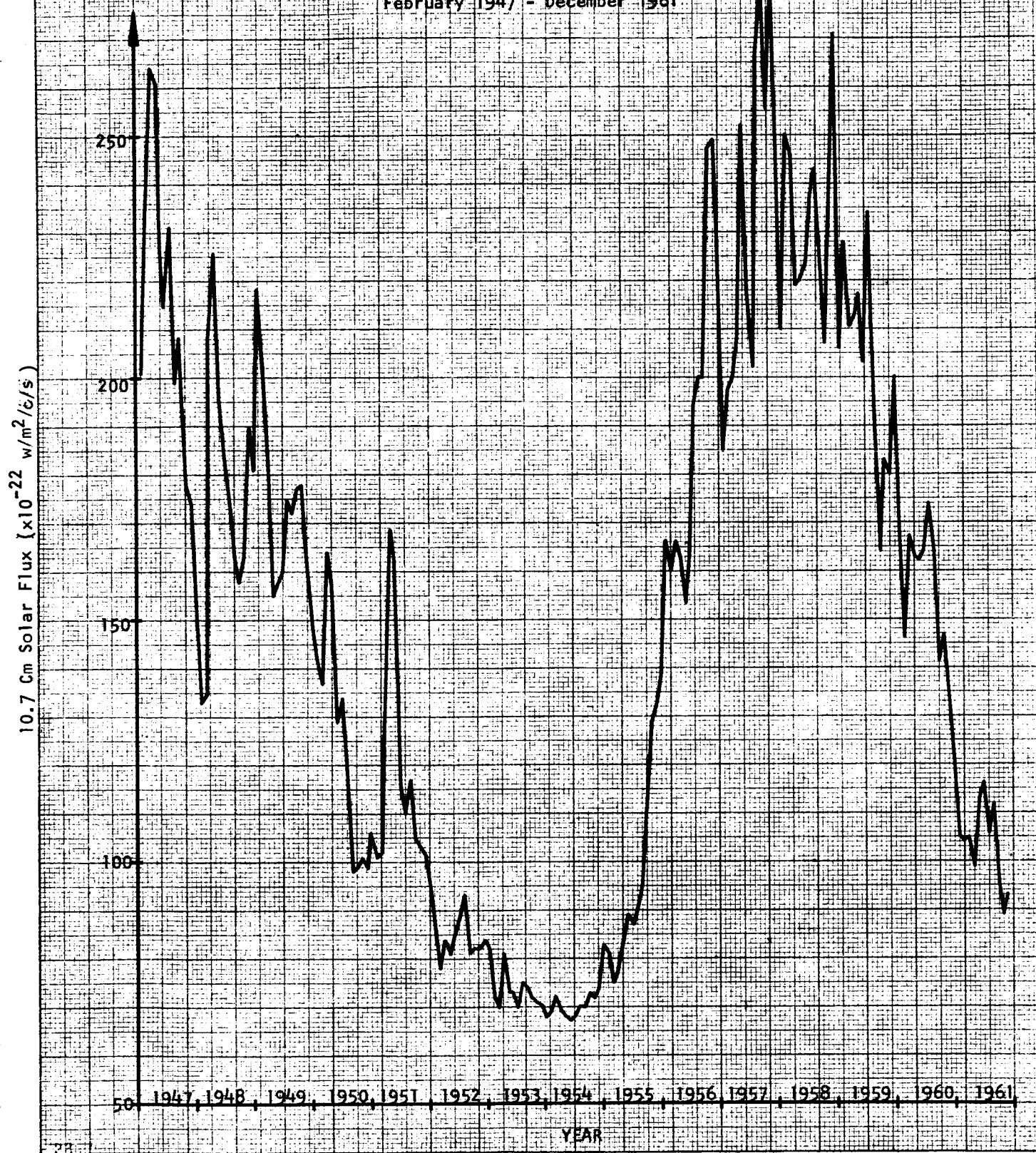
Fig. 6 Smoothed Mean Zurich Sunspot Numbers vs 2800 MC Radio Noise – February 1947 – December 1961

Sunspot
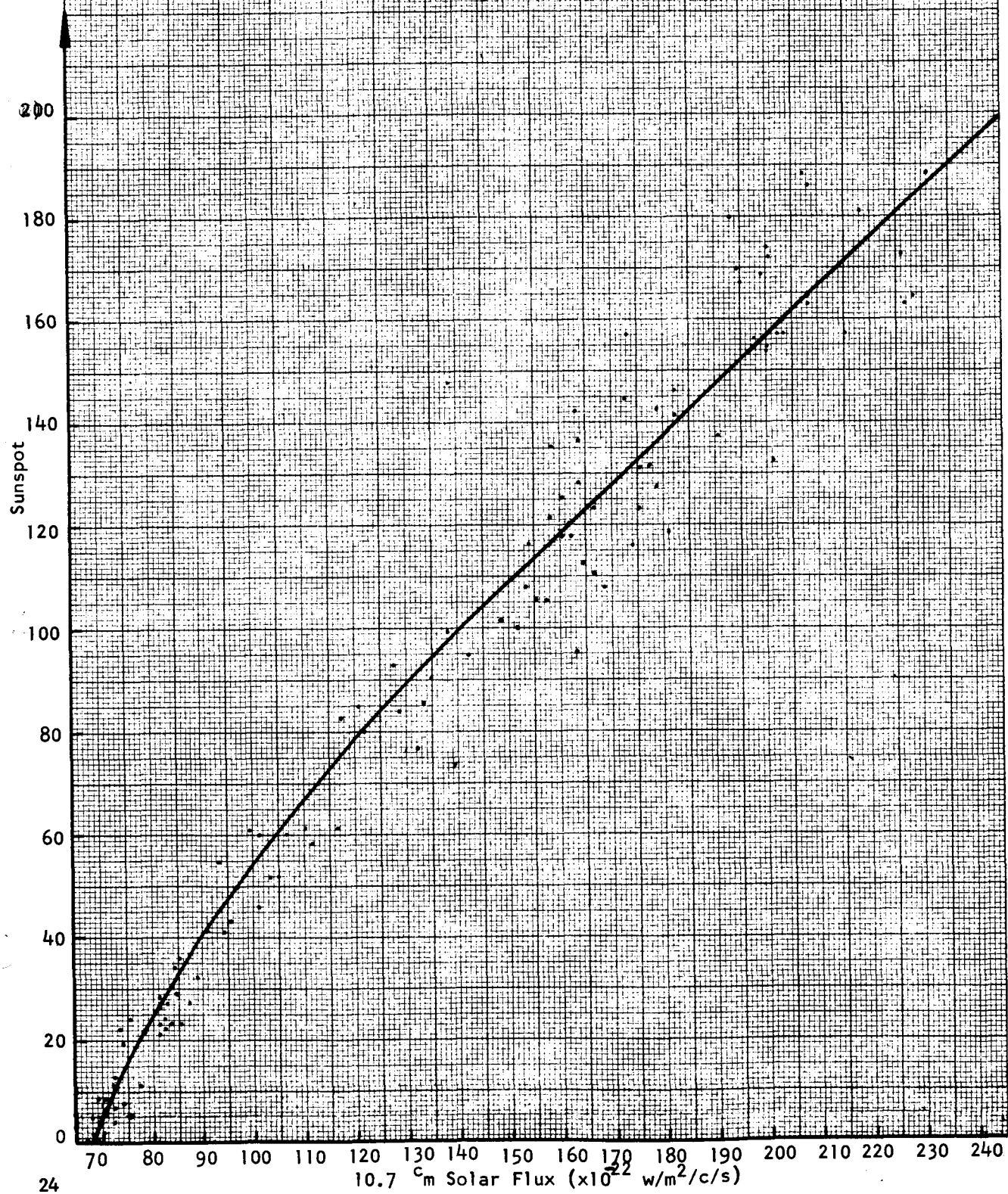
10.7 ^{c}m Solar Flux ($\times 10^{22}$ w/m^2/c/s)

Fig. 7. Density Variations at 200 and 600 Kilometers
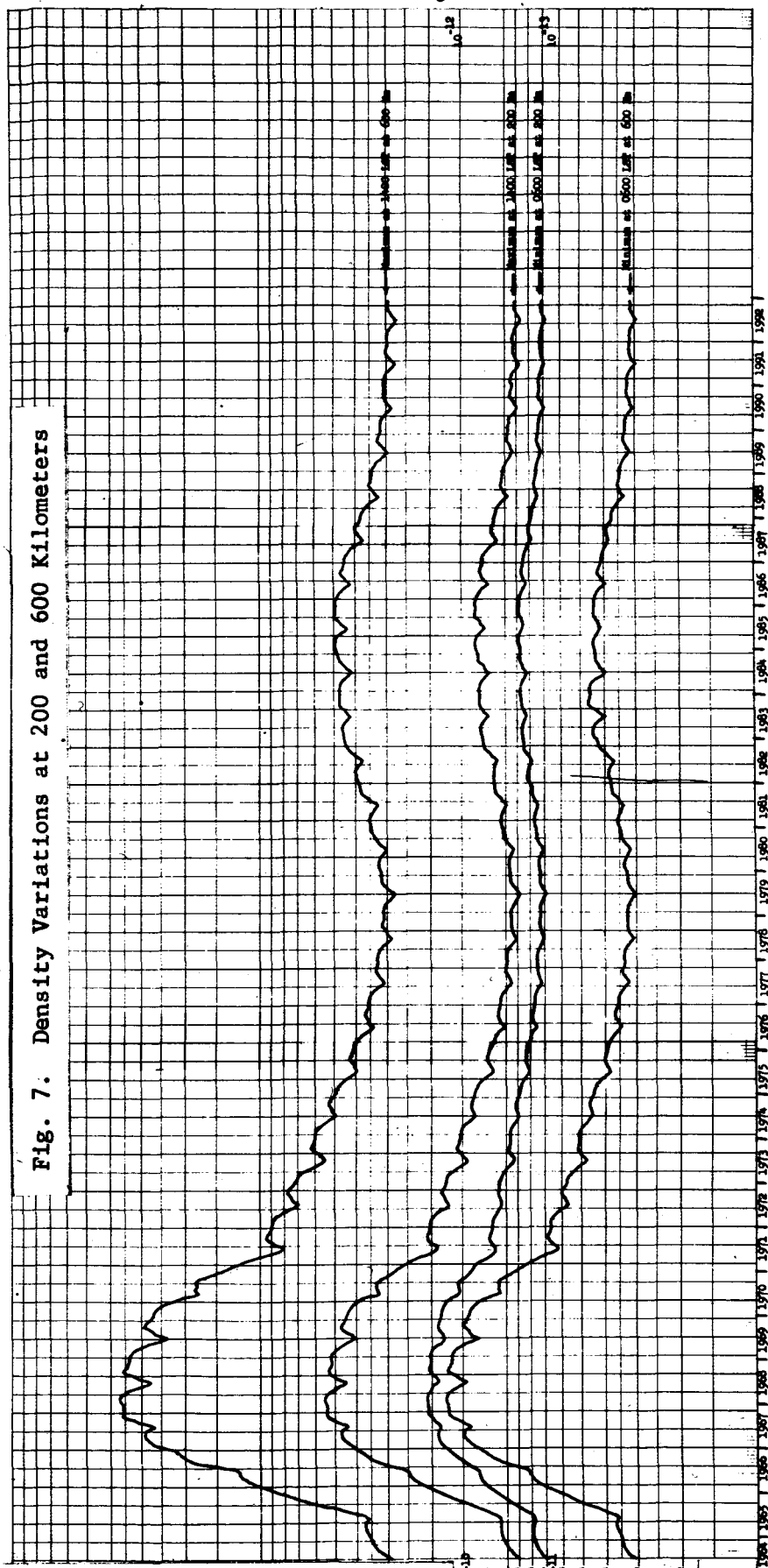
REFERENCES

1. Anderson, A. D., "A Simple Model for Atmospheric Density Variations from 200 to 800 KM," J. of Geophysical Research 19(3): 207-217, May 1962.

2. Anderson, A. D., "On the Inexactness of the 10.7 cm Flux from the Sun as an Index of the Total Extreme Ultaviolet Radiation," J. of the Atmospheric Sciences 21(1): 1-14, January 1964.

3. Champion, K. S. W., "Atmospheric Structure and Its Variations in the Lower Thermosphere," June 1963, Upper Atmosphere Physics Laboratory, Air Force Cambridge Research Laboratories, L. G. Hanscom Field, Massachusetts.

4. Chernosky, E. J. and M. P. Hagan, "The Zurich Sunspot Number and Its Variations for 1700-1957," J. of Geophysical Research 63(4): 775-788, 1958.

5. Das Gupta, M. K. and D. Basu, "Effect of the Earth's Orbital Eccentricity on Incident Solar Flux at 10.7 cm.," J. of Atmospheric and Terrestrial Physics 26: 135-137, 1964: Pergamon Press Ltd. Printed in Northern Ireland.

6. Harris, I. and R. Jastrow, "An Interim Atmosphere Derived from Rocket and Satellite Data," Planetary and Space Science 1:20-26, 1959: Pergamon Press, Printed in Great Britian.

7. Harris, I. and W. Priester, "Theoretical Models for the Solar Cycle Variation of the Upper Atmosphere," NASA TM X-640-62-70, June 1962, Goddard Space Flight Center, Greenbelt, Maryland.

8. Harris, I. and W. Priester, "Relation Between Theoretical and Observational Models of the Upper Atmosphere," J. of Geophysical Research 68(20):5891-5894, October 15, 1963.

9. Harris, I. and W. Priester, "Time Dependent Structure of the Upper Atmosphere," J. of the Atmospheric Sciences 19:286-301, July 1962.

10. Jacchia, L. G., "Atmospheric Structure and Its Variations at Heights above 200 km," Report to COSPAR Working Group IV (International Reference Atmosphere) presented at Fourth International Space Science Symposium, Warsaw, Poland, June 3 through 11, 1963.

11. Jacchia, L. G., "A Variable Atmospheric Density Model from Satellite Accelerations," J. of Geophysical Research 65(9): 2775-2782, September 1960.

26

REFERENCES (Continued)

12. Johnson, F. S., "Atmosphere Structure," Astronautics 7(8); 54-61, Aug 1962.

13. Kallmann, H. K., "A Preliminary Model Atmosphere Based on Rocket and Satellite Data," RAND Report 339, the RAND Corporation.

14. Kallmann-Bijl, H. K., "Daytime and Nighttime Atmospheric Properties Derived from Rocket and Satellite Observations," J. of Geophysical Research 66(3): 787-795, March 1961.

15. Kallmann-Bijl, H. K., "Variations of Atmospheric Properties with Time and Solar Activity," J. of Atmospheric and Terrestrial Physics 24: 831-841, 1962: Pergamon Press Ltd. Printed in Northern Ireland.

16. Kallmann-Bijl, H. K., and W. L. Sibley, "Diurnal Variation of Temperature and Particle Density Between 100 Km and 500 Km," Planetary and Space Science 11: 1379-1394, 1963: Pergamon Press Ltd. Printed in Northern Ireland.

17. King-Hele, D. G. and J. M. Rees, "The Decrease in Upper Atmosphere Density Between 1957 and 1963 as Revealed by Satellite Orbits," Royal Aircraft Establishment Technical Note No. Space 32, May 1963. Ministry of Aviation, London, W.C.2.

18. Martin, H. A., W. Neveling, W. Priester and M. Roemer, "Model of the Upper Atmosphere from 130 through 1600 Km, Derived from Satellite Orbits," Mitt. Sternwarte Bonn 35, COSPAR Symposium, Florence, Italy, 1961.

19. Nicolet, M., "Structure of the Thermosphere," Planetary and Space Science 5: 1-32, 1961: Pergamon Press. Printed in Great Britain.

20. Nicolet, M., "The Composition and Structure of the Terrestrial Atmosphere," Ionospheric Research Scientific Report No. 185, May 15, 1963, Ionosphere Research Laboratory, The Pennsylvania State University.

21. Nicolet, M., "A Representation of the Terrestrial Atmosphere from 100 Km to 3000 Km," Ionospheric Research Scientific Report No. 155, February 1962, Ionosphere Research Laboratory, The Pennsylvania State University.

REFERENCES (Continued)

22. Nicolet, M., "Solar Radioflux and Upper Atmosphere Temperature,"
Ionospheric Research Scientific Report No. 195, October 1, 1963,
Ionosphere Research Laboratory, The Pennsylvania State University.

23. Paetzold, H. K. and Zschorner, H., "An Annual and a Semiannual
Variation of the Upper Air Density," In Proceedings COSPAR
Symposium, Nice, France, 1960; North-Holland Printing Company,
Amsterdam (1960).

24. Priester, W., "Solar Activity Effect and Diurnal Variation in the
Upper Atmosphere," J. of Geophysical Research 66(12): 4143-4148,
December 1961.

25. Priester, W., H. A. Martin, and K. Kramp, "Diurnal and Seasonal
Density Variations in the Upper Atmosphere," Nature 189: 202-204,
October 15, 1960.

26. Schilling, G. F. and C. A. Whitney, "Derivation and Analysis of
Atmospheric Density from Observations of Satellite 1958 Epsilon,"
Planetary and Space Science1: 136-145, 1959: Pergamon Press.
Printed in Great Britain.

27. Singer, S. F., "Properties of the Upper Atmosphere and Their Rela-
tion to the Radiation Belts of the Earth," Planetary and Space
Science 2: 165-173, 1960: Pergamon Press. Printed in Great Britain.

28. Wasko, P. E. and T. A. King., "Earth's Aerospace Properties from
100 to 100,000 Km Altitude (Preliminary)," Geo. C. Marshall Space
Flight Center MTP-AERO-63-2, January 3, 1963.
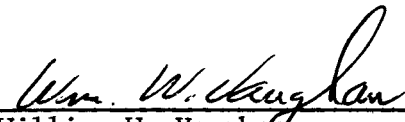
June 10, 1964   APPROVAL   NASA TM X-53062

AN AUTOMATED MODEL FOR PREDICTING AEROSPACE DENSITY BETWEEN
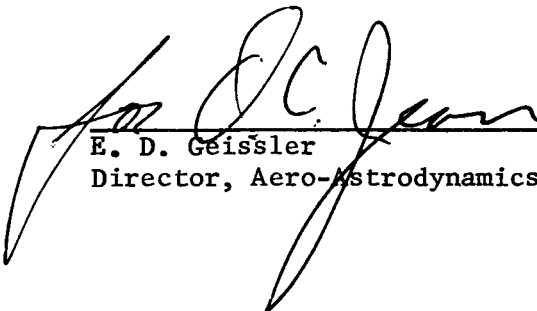200 AND 60,000 KILOMETERS ABOVE THE SURFACE OF THE EARTH

By Robert E. Smith

The information in this report has been reviewed for security
classification. Review of any information concerning Department of
Defense or Atomic Energy Commission programs has been made by the MSFC
Security Classification Officer. This report, in its entirety, has
been determined to be unclassified.

This document has also been reviewed and approved for technical
accuracy.

William W. Vaughan
Chief, Aero-Astrophysics Office

E. D. Geissler
Director, Aero-Astrodynamics Laboratory

29

DISTRIBUTION

DEP DIR
  Dr. E. Rees

R-DIR
  Mr. Weidner

R-SA
  Dr. Kuettner

R-FP
  Dr. Koelle
  Dr. H. O. Ruppe (2)

R-AERO
  Dr. E. D. Geissler
  Mr. O. C. Jean
  Dr. F. A. Speer
  Mr. F. O. Kurtz (3)
  Mrs. A. McNair
  Mr. J. Lindberg
  Dr. R. E. Hoelker
  Mr. William Miner
  Mr. H. J. Horn
  Mr. C. Baker
  Mr. J. Lovingood
  Mr. R. Ryan
  Mr. M. Rheinfurth
  Mr. W. Dahm
  Mr. E. Linsley
  Mr. H. Wilson
  Mr. J. Clark
  Mr. W. W. Vaughan (3)
  Mr. O. H. Vaughan
  Mr. R. E. Smith (20)
  Mr. O. E. Smith (2)
  Mr. J. R. Scoggins
  Mr. G. Daniels
  Mr. J. Kaufman
  Mr. C. Dalton
  Dr. W. Heybey
  Mr. William Murphree
  Dr. H. Sperling

MS-T
  Mr. Roy Bland

CC-P

HME-P
30

R-P&VE
  Mr. F. C. Cline
  Mr. E. Hellebrand
  Dr. H. G. Krause
  Mr. E. Goerner (2)

R-COMP
  Dr. H. Hoelzer (2)
  Miss Sylvia Bowers

R-RP
  Dr. E. Stuhlinger (2)
  Dr. W. Johnson
  Dr. R. D. Shelton

R-ASTR
  Dr. W. Haeussermann (2)
  Mr. O. Hoberg

R-LVO
  Dr. H. Gruene

I-DIR
  Mr. R. B. Young

NASA Headquarters

Office of Space Sciences & Application
  Dr. Homer Newell
  Dr. Morris Tepper (2)
  Mr. William Spreen
  Mr. M. Dubin (4)

Office of Advanced Research & Technology
  Dr. R. L. Bisplinghoff
  Mr. Hildred Chesley
  Dr. H. Kurzweg
  Mr. Milton Ames

Office of Tracking & Data Acquisition
  Mr. E. Buckley

MS-IP

MS-IPL (8)

MS-H

Office of Manned Space Flight
  Dr. George Muller
  Capt. R. F. Freitag
  Mr. Clyde Bothmer
  Dr. George M. Knauf
  Mr. Edward Gray
  Dr. Willis Foster

Kennedy Space Center
  Dr. K. Debus
  Dr. H. Knothe (2)

Goddard Space Flight Center
  Dr. Harry Goett
  Mr. William Stroud
  Dr. William Nordberg
  Mr. N. Spencer
  Dr. R. Jastrow
  Dr. W. Priester
  Mr. Herman LaGow
  Technical Library

Langley Research Center
  Director
  Mr. Richard Hord
  Mr. H. B. Tolefson
  Technical Library
  Mr. W. J. O'Sullivan

Manned Spacecraft Center
  Director
  Mr. J. M. Eggleston (2)
  Mr. M. A. Faget
  Mr. John Mayer
  Technical Library

Air Force Cambridge Research
  Laboratories
L. G. Hanscom Field
Bedford, Massachusetts
ATTN: Dr. K. S.W. Champion
      Dr. Norman W. Rosenberg
      Mr. A. Cole
      Mr. N. Sissenwine
      Technical Library

Air Weather Service
U. S. Air Force
Scott AFB, Illinois
ATTN: Commander (2)
      Dr. Robert Fletcher
      Mr. Roderiel Quiroz
      Maj. L. L. DeVries

Director
National Center For Atmospheric Research
Boulder, Colorado

Dr. Robert White, Chief (2)
U. S. Weather Bureau
Washington, D. C.

Dr. Luigi Jacchia
Smithsonian Institution
Astrophysical Observatory
Cambridge, Massachusetts

Army Missile Command
Redstone Arsenal, Alabama
ATTN: Technical Library (2)
     Dr. O. Essenwanger

Dr. G. F. Schilling
Dr. H. K. Kallmann-Bijl
The Rand Corporation
1700 Main Street
Santa Monica, California

Dr. Sidney Tewles
U. S. Weather Bureau
Washington, D. C.

Scientific and Technical Information
  Facility (25)
Attn: NASA Representative (S-AK-RKT)
     P. O. Box 5700
     Bethesda, Maryland